Supertoughening in B1 transition metal nitride alloys by increased valence electron concentration

Davide Giuseppe Sangiovanni, Lars Hultman and Valeriu Chirita

Original Publication:

Davide Giuseppe Sangiovanni, Lars Hultman and Valeriu Chirita, Supertoughening in B1 transition metal nitride alloys by increased valence electron concentration, 2011, Acta Materialia, (59), 5, 212-2134.
http://dx.doi.org/10.1016/j.actamat.2010.12.013

Supertoughening in B1 Transition Metal Nitride Alloys by Increased Valence Electron Concentration

D. G. Sangiovanni[a], L. Hultman[b], V. Chirita[c]

Thin Film Physics, Department of Physics, Chemistry and Biology (IFM), Linköping University, SE-581 83 Linköping, Sweden

e-mails: [a]davsan@ifm.liu.se, [b]larhu@ifm.liu.se, [c]vio@ifm.liu.se

Corresponding author: Davide G. Sangiovanni, Tel. 0046 13282623, Fax 0046 13137568

Abstract

We use density functional theory calculations to explore the effects of alloying cubic TiN and VN with transition metals *M* = Nb, Ta, Mo, W in 50% concentrations. The obtained ternaries are predicted to become supertough as they are shown to be harder and significantly more ductile compared to the reference binaries. The primary electronic mechanism of this supertoughening effect is shown in a comprehensive electronic structure analysis of these compounds to be the increased valence electron concentration intrinsic to these ternaries. Our investigations reveal the complex nature of chemical bonding in these compounds, which ultimately explains the observed selective response to stress. The findings presented in this paper thus offer a design route for the synthesis of supertough transition metal nitride alloys via valence electron concentration tuning.

Keywords: Nitrides; Mechanical properties; Ductility; *ab initio* calculations;

1. Introduction

Transition metal nitride alloys are well known for their excellent properties such as high hardness and wear resistance, high melting temperature, and good chemical inertness [1-3]. Among various technological applications, they are employed as protective coatings, in the cutting tool industry, to extend tools life and improve machining performances. To develop thin film nitride alloys with suitable mechanical and physical properties, material chemical composition can be tuned, and growth and processing parameters optimized, to control stoichiometry, microstructure, and texture. For protective coatings, high hardness is obviously a very sought after characteristic [4-8], as it prevents the surface from being scratched and worn at extreme working pressures. Typically, hardness enhancement is achieved by hindering the dislocations mobility, and hence reducing the plastic deformations in a material [9, 10]. Nevertheless, hardness improvements are often accompanied by embrittlement, which beyond a certain load results in film cracking. To achieve tools durability at various operating conditions, it is therefore necessary to design hard coating materials with enhanced ductility.

Previous studies have shown that it is possible to attain relatively ductile, yet hard materials. For instance, in non-isostructural superlattices [11], the alternating layers of ceramic B1-transition metal nitrides and more-ductile *bcc* metals, yield varying rates of plasticity while retaining hardness. Similarly, the nanocomposite structures developed by Voevodin and Zabinski [12], are designed to be hard at stresses below the elastic strength limit, while at extreme loading, their mechanical behavior switches to ductile, thus preventing brittle failure. In transition metal nitride alloys, the common approach to tailor mechanical properties to applications requirements is to combine different metallic species and/or to vary their ratio. Although brittleness in these hard ceramics is an obvious issue, the few theoretical studies [13, 14] which prospected this problem were in fact confined to the analysis of the

calculated elastic constants values and their trends. Clearly, more rigorous electronic structure investigations are required to understand the mechanisms leading to an appropriate/improved hardness-to-ductility ratio, or toughness, in materials.

Recently [15], we reported on a supertoughening process in ordered B1 $Ti_{0.5}M_{0.5}N$, for *M* = Mo and W. In that study, we demonstrated that this effect stems from a pronounced layered electronic arrangement on the metal stacking, not observed in the binary (TiN), which allows for a selective response to strain, respectively shear deformations of the crystal. Such charge distribution is induced in the crystal by the substitution of Ti with Mo or W atoms, as the exceeding valence electrons in these elements enhance the occupation of d-t_{2g} metallic states. These results imply the possibility to control ductility trends in materials by tuning the electron population in the d-t_{2g} metallic states, and broaden the research perspectives in the quest for new supertough B1 transition metal nitride alloys.

In the present paper we investigate the mechanical properties of cubic-B1 $Ti_{0.5}M_{0.5}N$ and $V_{0.5}M_{0.5}N$ (*M* = V, Nb, Ta, Mo, W) by means of ab-initio density functional theory (DFT) calculations to identify candidate materials for potentially hard coatings with enhanced ductility. Primarily, this choice is based on our previous results for TiMoN and TiWN alloys [15], and the fact that the thin films containing combinations of these elements grown in the rocksalt structure have been reported to have comparable hardness to TiN and TiAlN [16-20]. In the alloys proposed herein, the metallic elements are selected so as to span the valence electron concentration (VEC) per unit formula from a minimum of 9 (in the reference material TiN), up to a maximum of 10.5 (in $V_{0.5}Mo_{0.5}N$), as beyond this value further filling of the d-t_{2g} metallic states might lead to the instability of the cubic phase [21]. Our elastic constants estimations show that, with increasing VEC, $Ti_{0.5}M_{0.5}N$ and $V_{0.5}M_{0.5}N$ are progressively less resistive to shear deformations, while retaining stiffness and very low compressibility. The electronic structure and crystal orbital overlap population (COOP) [22]

calculations reported herein indicate that the increasing VEC is a key factor in ductility enhancement in the ternaries studied. In addition, we analyze the stress-strain relationship in these alloys and find that the increase in VEC activates the $\{110\}\langle 1\bar{1}0\rangle$ slip system, and promotes dislocation motion. Furthermore, our hardness estimations obtained using theoretical methods [23, 24], are in good agreement with indentation measurements and suggest that all these crystalline phases are excellent candidates for the synthesis of supertough B1 transition metal nitride alloys.

2. Computational details

The DFT calculations reported herein are performed with the Vienna *ab-initio* simulation package (VASP) [25] in the generalized gradient approximation of Perdew-Wang (GGA-PW91) [26], and the electron-ion interactions are described by the projector augmented wave potentials (PAW) [27]. In all calculations we use a large energy cutoff of 500 eV for the plane-wave basis to achieve total energy convergence within 10^{-5} eV. Structure relaxations are carried out with 4x4x4 **k**-points grids, while density of states (DOS), charge density distribution, and COOP are computed with 8x8x8 **k**-points grids in the Monkhorst-Pack scheme [28]. The supercells employed in our investigations contain 64 atoms with a minimum number of intermetallic bonds (C#3 structure) [15], closely matching the CuPt-type atomic ordering observed experimentally in $Ti_xW_{1-x}N$ films [29] and consistently found most stable energetically in our calculations. We compute for all alloys lattice constants *a*, bulk moduli *B*, elastic constants C_{11}, C_{12} and C_{44}, Young moduli *E*, shear moduli *G*, Poisson's ratios ν, and theoretical hardness *H*. The ideal lattice constant and the bulk modulus are evaluated by fitting the total energy-volume curve to the Birch-Murnaghan equation of state [30]. More details about elastic constants and related moduli calculations can be found in our previous report [15].

We assess the theoretical Knoop hardness H_k of all compounds, by using the semi-empirical method proposed by Šimůnek for covalent and ionic crystals [23]. For the structures employed in our calculations, in which nitrogen atoms (N) and metal atoms (*M*) are nearest neighbors, Šimůnek's formula becomes:

$$H_k = (C/\Omega)\sum_M b_{N,M} s_{N,M} \exp(-\sigma f_2), \quad (1)$$

in which $b_{N,M}$ accounts for the number of N – *M* interatomic bonds in a unit cell of volume Ω, while *C* (= 1450) and σ (= 2.8) are parameters fitted so that eq. (1) reproduces Knoop's hardness values (in GPa) for selected covalent and ionic crystals. The quantity $s_{N,M}$, called bond strength, is expressed as:

$$s_{N,M} = \sqrt{e_N e_M}\,/(n_N n_M d_{N,M}), \quad (2)$$

where *n* (= 6) is the coordination number, $d_{N,M}$ is the interatomic distance between N and *M*, and *e* is the ratio of the valence electrons number to the atomic radius value taken from Pearson's book [31]. Finally, the expression for f_2 is:

$$f_2 = \left(\frac{e_N - e_M}{e_N + e_M}\right)^2. \quad (3)$$

Furthermore, we use a recently reported method designed to predict the Vickers hardness in transition metal carbides and nitrides [24]. This parameter free approach involves the estimation, in addition to bond length, density and ionicity, of the intrinsic metallicity in the chemical bonds of these compounds from ab-initio calculations. The technique quantitatively reproduces the negative effect of *d* valence electrons on the hardness of primarily covalency-dominant binary transition metal carbides and nitrides, and is based on using Mulliken atomic and bond populations to estimate the different components in chemical bonds. According to

this formulation, the Vickers hardness H_v in binaries with a single type of M – N bond can be estimated using:

$$H_v = 1051 N_e^{2/3} d^{-2.5} \exp(-1.191 f_i - 32.2 f_m^{0.55}) \quad (4)$$

where N_e is the valence electron density defined as in the original paper [32] and d is the bond length. In the above formula, f_i and f_m, are the Phillips ionicity, respectively metallicity, of a chemical bond, and are used as correction factors to reflect the screening effects of ionic and metallic components on covalent bonds. The Phillips ionicity is defined as:

$$f_i = \left[1 - \exp\left(-|P_C - P|/P\right)\right]^{0.735} \quad (5)$$

with P as the overlap population of the bond and P_C the overlap population of a bond in a hypothetical pure covalent crystal with the same structure. Metallicity can be calculated as:

$$f_m = 0.026 D_F / n_e \quad (6)$$

with D_F as the electron density of states at the Fermi level and n_e the number of valence electrons per unit cell. For multicomponent compound systems, the hardness can be predicted as the average of hardness of all hypothetical binary systems in the respective compound:

$$H_v = \left[\prod^{\mu} \left(H_v^{\mu}\right)^{n^{\mu}}\right]^{1/\sum n^{\mu}} \quad (7)$$

where H_v^{μ} is the hardness of the hypothetical binary containing μ-type bonds and n^{μ} the number of μ-type bonds in the complex compound.

We calculate the charge density of crystal structures in real space using 132x132x132 grid points. This technique, which entails mapping the difference between self-consistent charge densities and charge densities derived from the superposition of atomic

wavefunctions, is thus useful in identifying the effects of shear deformations upon charge distribution in crystals, by tracing the charge transfer from initially non-interacting atomic orbitals into the chemical bonds of the final atomic configurations.

COOP calculations are generally used to investigate the binding character of chemical bonds in a crystal [22] by estimating the overlap population of molecular orbitals. The method resolves the bonding (positive values) and anti-bonding (negative values) contributions to covalent bonds, while absolute values are indicative of the bond strength. Herein we report the results of a COOP analysis based on VASP calculations using PAW potentials, known to compare very well in terms of accuracy with full-potential methods. With appropriate manipulation of VASP output data, COOP summations, for all interacting atom pairs in the calculation supercell, can be performed over all occupied states, and the resulting integrated COOP (ICOOP) measures the strength of a particular covalent bond in the crystal. We emphasize the fact that any such analysis provides no information on the ionic character of a bond. Consequently, COOP and ICOOP calculations should only be used to qualitatively estimate and/or compare bond strength in different compounds. In the present study, we use COOP and ICOOP primarily to assess the effects of strain/shear on the strength of a particular chemical bond, namely between pairs of first and second neighbors in the crystal.

Finally, to qualitatively assess the general trend in the response to deformations, we estimate the stress-strain relationship for a number of selected ternaries and compare it with the behavior of reference binaries. The stress-strain curves are obtained by relaxing all atomic positions and maintaining fixed supercell shapes, for each strain, in calculations using 8x8x8 **k**-points grids. Stress values in the direction of interest are then extracted from the stress tensor, directly from the VASP output. Several calculations with no constraints on shearing [33], i.e. allowing for cell shape relaxations in all directions except in the direction of applied

strain, were tested for TiN and $Ti_{0.5}W_{0.5}N$ at several strain values. Given the small differences in stress values obtained with the two approaches, under a few percent, the former method, less computationally expensive, was chosen in this study.

3. Results and discussion

Table 1 presents the results of our calculations for the binaries and ternaries studied in this paper. As it can be seen, the properties estimated herein for the two reference binaries, TiN and VN, are in very good agreement with previous experimental [1, 34-38] and *ab-initio* [13, 39-43] results, shown in Table 2. Not surprisingly, crystal properties data for $Ti_{0.5}M_{0.5}N$ and $V_{0.5}M_{0.5}N$ is sparse, and a direct comparison with our predictions is thus not possible. Nonetheless, our estimations for the lattice constants of $Ti_{0.5}M_{0.5}N$ alloys match within 1% the available experimental results [29, 44-48], as shown in Table 3. In addition to the solid agreement with previous data for TiN and VN, the results in Table 1 are indicative of another interesting trend. Namely, the alloying of both binaries with V (TiN only), Nb, Ta, Mo and W, corresponding to an increase in valence electron concentration (VEC) from 9 to 10.5 electrons per unit cell, has the following effects in the resulting ternaries: a continuous increases in bulk modulus values, accompanied by a continuous decrease in G and C_{44} values. We also note that on average, the alloys exhibit 20% lower Young's modulus values compared to the reference binaries.

As a first aspect of this trend in mechanical properties, we discuss the hardness of $Ti_{0.5}M_{0.5}N$ and $V_{0.5}M_{0.5}N$ alloys. In experiments, the hardness of a thin film is measured from indentation tests, in which different factors affect the result, such as texture, average grain size, stoichiometry, and lattice mismatch between film and substrate materials. While the addition of a second transition metal has indeed often been connected to hardness enhancements in B1-Ti*M*N [4-7], these findings may be due to film microstructure features

Table 1. Present work DFT estimations of elastic properties for binary and ternary nitrides.

	a (Å)	B (GPa)	E (GPa)	G (GPa)	C_{44} (GPa)	C_{11} (GPa)	C_{12} (GPa)	C_{12}-C_{44} (GPa)	G/B	ν
TiN[a]	4.254	290	489	200	159	640	115	-44	0.690	0.219
$Ti_{0.5}V_{0.5}N$	4.188	312	432	170	144	592	172	28	0.545	0.269
$Ti_{0.5}Nb_{0.5}N$	4.363	295	403	159	120	581	148	28	0.539	0.270
$Ti_{0.5}Ta_{0.5}N$	4.348	304	366	141	107	559	176	69	0.464	0.299
$Ti_{0.5}Mo_{0.5}N$[a]	4.300	321	382	147	77	655	153	76	0.458	0.302
$Ti_{0.5}W_{0.5}N$[a]	4.298	336	394	151	60	720	145	85	0.449	0.305
VN	4.121	320	478	191	139	680	140	1	0.597	0.251
$V_{0.5}Nb_{0.5}N$	4.304	301	399	156	100	621	141	41	0.518	0.279
$V_{0.5}Ta_{0.5}N$	4.291	313	379	146	73	653	143	70	0.466	0.298
$V_{0.5}Mo_{0.5}N$	4.250	333	340	128	71	617	191	120	0.384	0.330
$V_{0.5}W_{0.5}N$	4.246	340	372	141	61	690	166	105	0.415	0.318

a = Ref. [15]

Table 2. DFT data for TiN and VN, comparison with experimental and theoretical values.

	Present work	Ab-initio calculations	Experimental
TiN			
a (Å)	4.254[a]	4.221[b], 4.246[c], 4.270[d], 4.275[e]	4.240[h], 4.240[i]
B (GPa)	290[a]	270[b], 287[c], 292[d], 264[e], 295[f]	346[i], 318[j]
E (GPa)	489[a]	487[b], 456[c], 470[d], 514[f]	455[i], 475[j], 470[k], 590[l]
G (GPa)	200[a]	203[b], 189[c], 191[d], 213[f]	178[i], 190[j]
C_{44} (GPa)	159[a]	168[b], 165[c], 162[d], 166[f]	156[i], 163[j], 192[m]
C_{11} (GPa)	640[a]	610[b], 585[c], 604[d], 671[f]	626[i], 625[j]
C_{12} (GPa)	115[a]	100[b], 137[c], 136[d], 106[f]	206[i], 165[j]
ν	0.219[a]	0.199[b], 0.235[c], 0.230[d], 0.210[f]	0.281[i], 0.251[j]
VN			
a (Å)	4.121	4.128[d], 4.110[e], 4.132[g], 4.127[g]	4.140[h]
B (GPa)	320	320[d], 313[e], 326[f], 316[g], 310[g]	268[j]
E (GPa)	478	434[d], 441[f]	400[j], 460[l]
G (GPa)	191	170[d], 173[f]	160[j]
C_{44} (GPa)	139	126[d], 137[f]	133[j], 149[m]
C_{11} (GPa)	680	636[d], 652[f]	533[j]
C_{12} (GPa)	140	162[d], 163[f]	135[j]
ν	0.251	0.270[d], 0.270[f]	0.251[j]

REFERENCES TABLE 2

a = Ref. [15] b = Ref. [39] c = Ref. [40] d = Ref. [41] e = Ref. [42] f = Ref. [13] g = Ref. [43]
h = Ref. [1] i = Ref. [34] j = Ref. [35] k = Ref. [36] l = Ref. [37] m = Ref. [38]

Table 3. DFT calculated and experimental lattice parameters for ternary nitrides.

	Lattice constant (Å)	
	Present work	Exp.
$Ti_{0.5}V_{0.5}N$	4.188	4.19[b]
$Ti_{0.5}Nb_{0.5}N$	4.363	4.32[b], 4.41[c]
$Ti_{0.5}Ta_{0.5}N$	4.348	4.37[c], 4.31[d], 4.33[e]
$Ti_{0.5}Mo_{0.5}N$	4.300[a]	4.33[c], 4.25[f]
$Ti_{0.5}W_{0.5}N$	4.298[a]	4.28[c], 4.25[g]

a = Ref. [15] b = Ref. [46] c = Ref. [44] d = Ref. [47] e = Ref. [48] f = Ref. [45] g = Ref. [29]

rather than to an inherent hardness of perfect crystalline materials. To assess films hardness directly from DFT calculations would require too large supercells for the available computational time. Ab-initio methods [32, 49] may however be used indirectly to estimate the hardness of ideal crystals, by assuming that in the absence of defects the indented volume size is uniquely related to the resistance of the inner chemical bonds, and using first principles calculations to obtain the necessary information on the respective bonds. This is the manner in which parameters are fitted to reproduce Knoop's hardness values of covalent and ionic crystals [23, 49], and chemical bonds characterized to predict Vickers hardness for transition metal nitrides and carbides [24, 32]. Naturally, growth and processing conditions affect the actual film microstructure, which ultimately is significantly different to the defect-free crystals models. In spite of this aspect, and of the disputed merits and limits of theoretical approaches [50, 51], the methods for ideal crystals can be used to relatively assess the potential hardness of $Ti_{0.5}M_{0.5}N$ and $V_{0.5}M_{0.5}N$ alloys, since the comparison with same type calculations for binaries and compounds well studied experimentally, yields at least a qualitative trend of the hardness of these ternaries.

In Table 4, the calculated hardness values of compounds studied in this paper are listed and compared, where possible, with Knoop [16-20, 52] and Vickers/Berkovich [4-7, 36, 48, 53-59] indentation results. As expected perhaps, calculations are generally in good agreement with the respective experimental tests. It is also interesting to note that theoretical predictions systematically underestimate the hardness of most compounds. Significantly, the experimental results obtained with either method, demonstrate that the hardness of all Ti*M*N alloys is higher than that of TiN. Though in different compositions compared to experiments, these findings are confirmed by our calculations for $Ti_{0.5}M_{0.5}N$. We find the same trend for $V_{0.5}M_{0.5}N$ with respect to VN, and more importantly, V ternaries are generally predicted to have higher hardness values compared to Ti ternaries. While the available experimental data on V ternaries does not allow for direct verification of these observations, the arguments presented above demonstrate that the Ti and V ternaries studied herein have a hardness which is at least comparable to, if not significantly higher than, that of materials generally accepted as hard compounds.

The other notable feature of the results in Table 1, as already discussed, is the continuous decrease in G and C_{44} values with increasing VEC in the ternaries obtained by alloying the reference binaries. This tendency obviously affects a number of properties in any material, among which the G/B ratio, the Cauchy pressure (C_{12} - C_{44}) and the Poisson ration. In the present study the former two quantities are most significant, as it is well known that they are the main criteria for assessing ductility of materials. As in our previous report [15], here we use the same Pugh [60] and Pettifor [61] criteria, to map the ductility trend of the ternaries studied. These results are shown in Fig. 1, and it can easily be observed that almost without exception, alloying has the effect of significantly enhancing ductility in all cases studied. The only compounds which are not within the ductile region of the map are the Nb ternaries and $Ti_{0.5}V_{0.5}N$, yet one can clearly see that even in these situations ductility is enhanced compared

Table 4. Predicted hardness values and experimental results obtained in Knoop and Vickers/Berkovich indentation tests.

	Hardness (GPa)				
	Knoop		Vickers/Berkovich		
	Theor.	Exp.	Theor.		Exp.
TiN	16.6	17.7[a], 21.2[b] ($TiN_{0.91}$), 10.7[c], 11.7[d]	21.7[*]	21.6[**]	19-21[g], 17.2[h], 21.6[i], 26[j] ($TiN_{0.9}$)
$Ti_{0.5}Al_{0.5}N$	15.0	24.4[c], 19.4[d], 17.3[e] ($Ti_{0.43}Al_{0.57}N$)	29.4[*]	21.7[**]	27.8-30.4[k]
$Ti_{0.5}V_{0.5}N$	21.5	23.0[e], 23.5[f] ($Ti_{0.5}V_{0.5}N_y$, $0.7<y<0.85$)	25.2[*]	18.0[**]	20.0[i], 23.1[l] ($Ti_{0.43}V_{0.57}N$)
$Ti_{0.5}Nb_{0.5}N$	17.3		26.9[*]	17.1[**]	24.7[m] ($Ti_{0.3}Nb_{0.7}N_{0.7}$), 40[n], 50[n]
$Ti_{0.5}Ta_{0.5}N$	17.5	25.6[e] ($Ti_{0.68}Ta_{0.32}N$)	20.4[*]	20.8[**]	31[o]
$Ti_{0.5}Mo_{0.5}N$	21.1	23.7[b] ($Ti_{0.54}Mo_{0.46}N_{0.84}$)	25.9[*]	15.9[**]	34.4[p] ($Ti_{0.52}Mo_{0.48}N$)
$Ti_{0.5}W_{0.5}N$	21.1	24.7[e] ($Ti_{0.66}W_{0.34}N$), 32.6[e] ($Ti_{0.36}W_{0.64}N$)	27.3[*]	17.6[**]	33[q] ($Ti_{0.6}W_{0.4}N$), 40[r] ($Ti_{0.3}W_{0.7}N$)
VN	27.2	24.0[f] (VN_y, $0.62<y<0.66$)	16.2[*]	14.9[**]	15.9[i], 14.5-25.2[s] (VN_y, $0.81<y<0.91$)
$V_{0.5}Nb_{0.5}N$	21.8		18.1[*]	14.2[**]	18.2[h] ($V_{0.6}Nb_{0.4}N$)
$V_{0.5}Ta_{0.5}N$	22.1		17.5[*]	17.3[**]	
$V_{0.5}Mo_{0.5}N$	25.8		24.9[*]	13.2[**]	
$V_{0.5}W_{0.5}N$	25.9		24.1[*]	14.6[**]	

[*] Values obtained using general definition in equation (4) and overlap populations calculated in this work, as used for the COOP analysis.
[**] Values obtained using average formulation in equation (7) and overlap populations of hypothetical binaries published in original paper [24].

REFERENCES TABLE 4

a = Ref. [16] b = Ref. [17] c = Ref. [20] d = Ref. [52] e = Ref. [18] f = Ref. [19] g = Ref. [54] h = Ref. [53] i = Ref. [59] j = Ref. [36] k = Ref. [56] l = Ref. [7] m = Ref. [58] n = Ref. [4] o = Ref. [48] p = Ref. [6] q = Ref. [5] r = Ref. [55] s = Ref. [57]

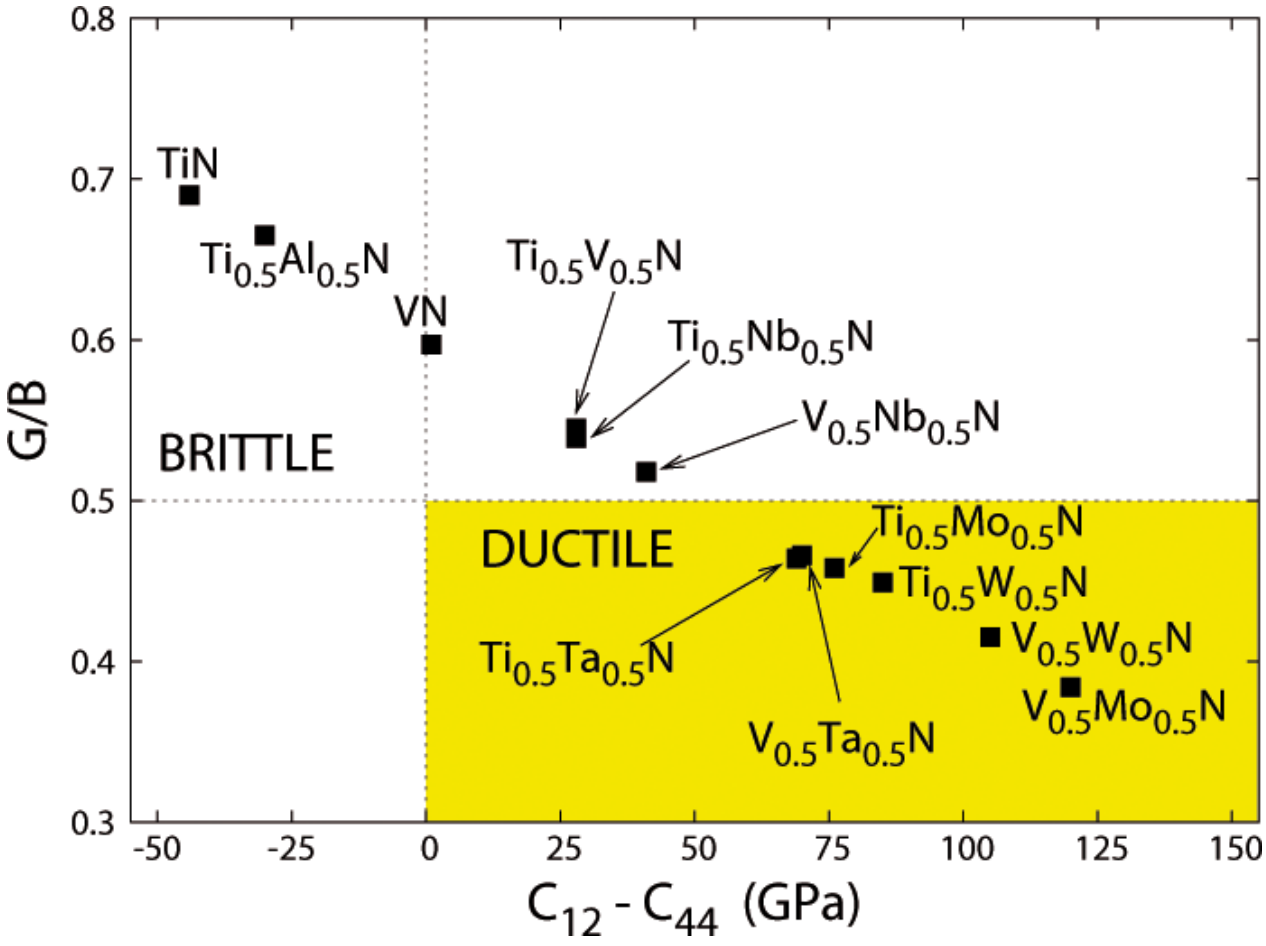

Fig. 1. (Color online) Map of brittleness and ductility trends in compounds as estimated in this work.

to the reference binaries ($Ti_{0.5}Al_{0.5}N$ is included here only as a brittleness reference point). In conjunction with the predicted hardness improvement discussed above, the demonstrated ductility enhancement for these ternaries confirms that the supertoughening effect reported for TiMoN and TiWN is operating in all ternaries analyzed herein. In addition, the data in

Fig. 1 indicates that this effect is more pronounced with increasing VEC, and the best results are obtained for *M* = Mo or W, i.e. for VEC values of 10 and 10.5 electrons per unit cell.

To verify the above assertion, we investigate the electronic structure of these ternaries and compare it with that of compounds for which the toughness enhancement mechanism has been explained [15]. For practical and clarity reasons, the discussion in the present study concentrates on the comparison between $Ti_{0.5}W_{0.5}N$ and $V_{0.5}W_{0.5}N$, primarily by analyzing the effects of shearing upon chemical bonding in the two compounds. Nevertheless, an analogous argumentation can be formulated for each alloying case in this study, so the general conclusions are valid for all ternaries considered herein.

The starting point in this comparison is the examination of the overall charge density distributions in $Ti_{0.5}W_{0.5}N$ and $V_{0.5}W_{0.5}N$, of the unstrained, respectively shear strained structures. The results are shown in Fig. 2, and as it can be easily seen, there is an obvious similarity between the charge density profiles of $Ti_{0.5}W_{0.5}N$ (top panels) and $V_{0.5}W_{0.5}N$ (lower panels), in both the unstrained (Figs. 2a and 2c) and strained (Figs. 2b and 2d) situations. Evidently, the addition of W in VN has the same effect as in TiN, which is to delocalize the charge in the vicinity of W nuclei, leading to the formation of a layered electronic structure upon shearing, consisting in alternating layers of high/low charge concentration along the $[1\,\bar{1}\,0]$ direction [15]. As shown in that report, this layered electronic structure is the result of increased VEC in ternaries (one more valence electron per unit cell compared to reference binaries), which in turn increases the occupancy of *d*-t_{2g} metallic states, due to increased overlapping of these orbitals upon shearing.

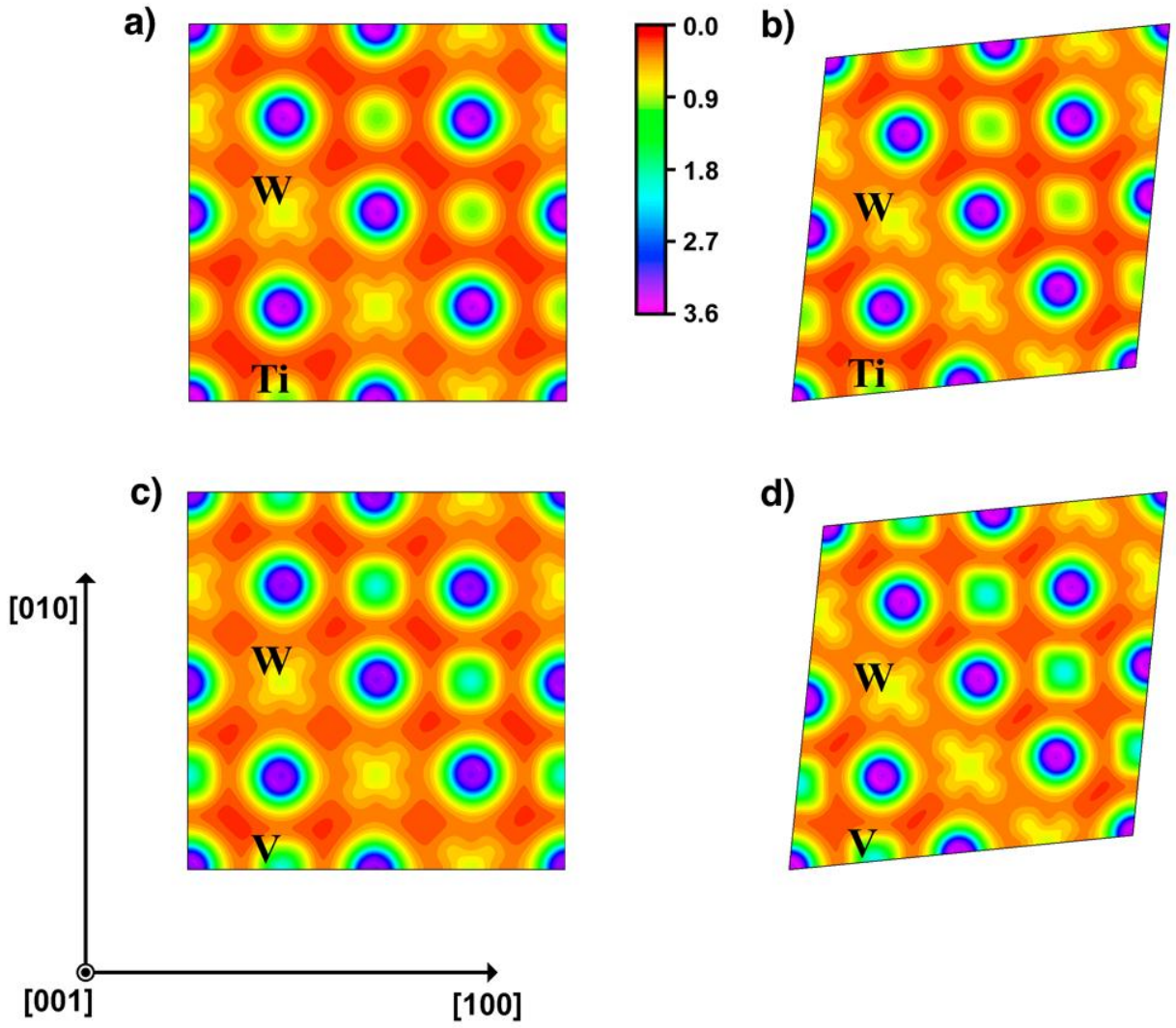

Fig. 2. (Color online) Charge densities of $Ti_{0.5}W_{0.5}N$ (upper panels) and $V_{0.5}W_{0.5}N$ (lower panels) for: (a) and (c) unstrained structures; (b) and (d) shear strained (10%) configurations. Color scale units are electrons/Å^3.

In order to further probe the VEC ductility enhancement effects in these ternaries, a deeper analysis of the relationship between strain and bonding in these materials is required. We start by comparing the partial DOS of unstrained and strained $Ti_{0.5}W_{0.5}N$ configurations to observe the *d*-states response to 5% and 10% trigonal deformations. As it can be seen in Fig. 3a, as shear strain increases, the populated *d*-e_g states are destabilized and progressively shift to higher binding energies. This is an expected tendency in ternary nitrides as the *p*(N) – *d*-e_g(Ti,W) states account primarily for 1st neighbor interactions and have a pronounced covalent/directional character. It has in fact been shown that at a VEC of 8.4 electrons per

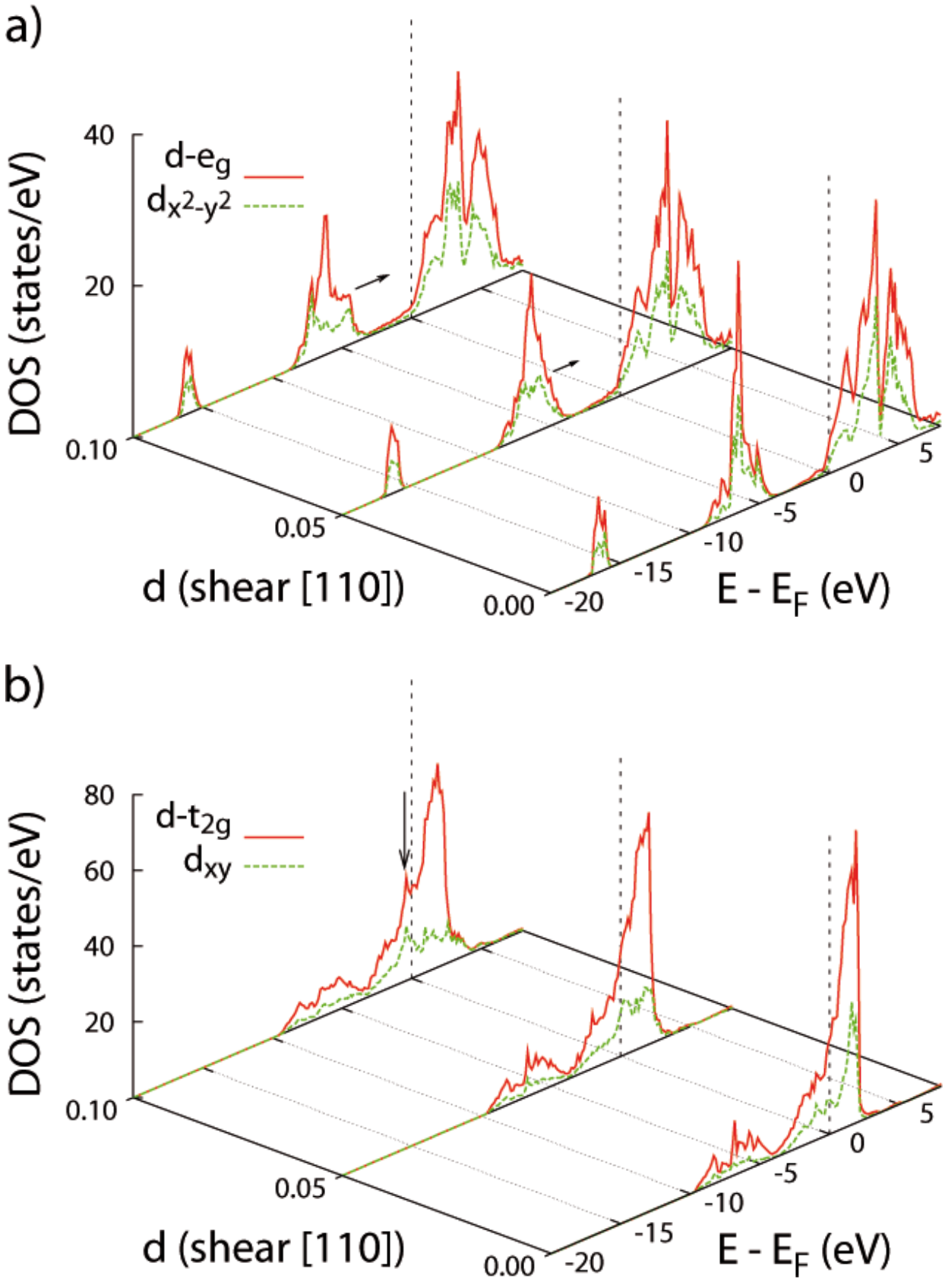

Fig. 3. (Color online) Shearing induced effects on the $Ti_{0.5}W_{0.5}N$ partial DOS at 0, 5 and 10% strains: (a) shifting of *d*-e_g states to higher energies and (b), increasing population of *d*-t_{2g} states.

unit cell, the p(N,C) – d-e_g(Ti) states are fully occupied, and yield the maximum hardness and C_{44} values in B1-$TiC_{1-x}N_x$ alloys [62]. Beyond the threshold of VEC = 8.4, which is the case here, valence electrons start filling the d-t_{2g} metallic states and can reduce hardness and shear resistance. This trend is visible in Fig. 3b, where one can see that with increasing strain, d-states with t_{2g} symmetry also shift to higher energies, however, at maximum strain, a clear secondary peak forms in the t_{2g} – DOS just below the Fermi level. The lower curves in Fig. 3b (green online) also suggest this peak is mainly induced by an enhanced occupancy of d_{xy} states. As reported, [15, 62], such electronic response to [110] shear deformations may stem from the shortening of metal-metal, 2nd neighbor distance along the $[1\,\bar{1}\,0]$ direction, favoring $d_{xy} – d_{xy}$ orbitals overlapping. Similar changes are expected in the electronic structures of the other ternaries considered here, as illustrated by the comparison shown in Fig. 4, where one can see the analogous d-t_{2g} states response to shearing in $V_{0.5}W_{0.5}N$ (lower panels) closely matching that in $Ti_{0.5}W_{0.5}N$ (top panels).

In order to better illustrate the changes induced in chemical bonding upon shearing, we plot in Fig. 5 the results of our COOP analysis, typically used to assess modifications in covalent bonding. Fig. 5a shows the COOP results for $Ti_{0.5}W_{0.5}N$ obtained from M – N orbitals overlapping. We note that our $Ti_{0.5}W_{0.5}N$ VASP-based COOP calculations for the unstrained configuration are in good agreement with those obtained using the full-potential linear muffin-tin orbital method for TiN/TiC [63]. The two bonding peaks, located close to -7 and -18 eV, correspond to p(N) – d-e_g(M) and s(N) – s(M) σ orbitals, i.e. essentially 1st neighbor interactions. As strain increases, one can observe a pronounced decrease in the peak close to -7 eV (green curve online), suggestive of the significant weakening in the M – N bonds induced during trigonal deformations. A totally different situation is observed in Fig. 5b, which depicts the COOP results corresponding to 2nd neighbor interactions, obtained from d-t_{2g}(M) – d-t_{2g}(M) orbitals overlapping. Here, in correlation with the DOS results presented

in Fig. 3b, bonding d-t_{2g} – d-t_{2g} states are clearly formed below the Fermi energy level as strain increases.

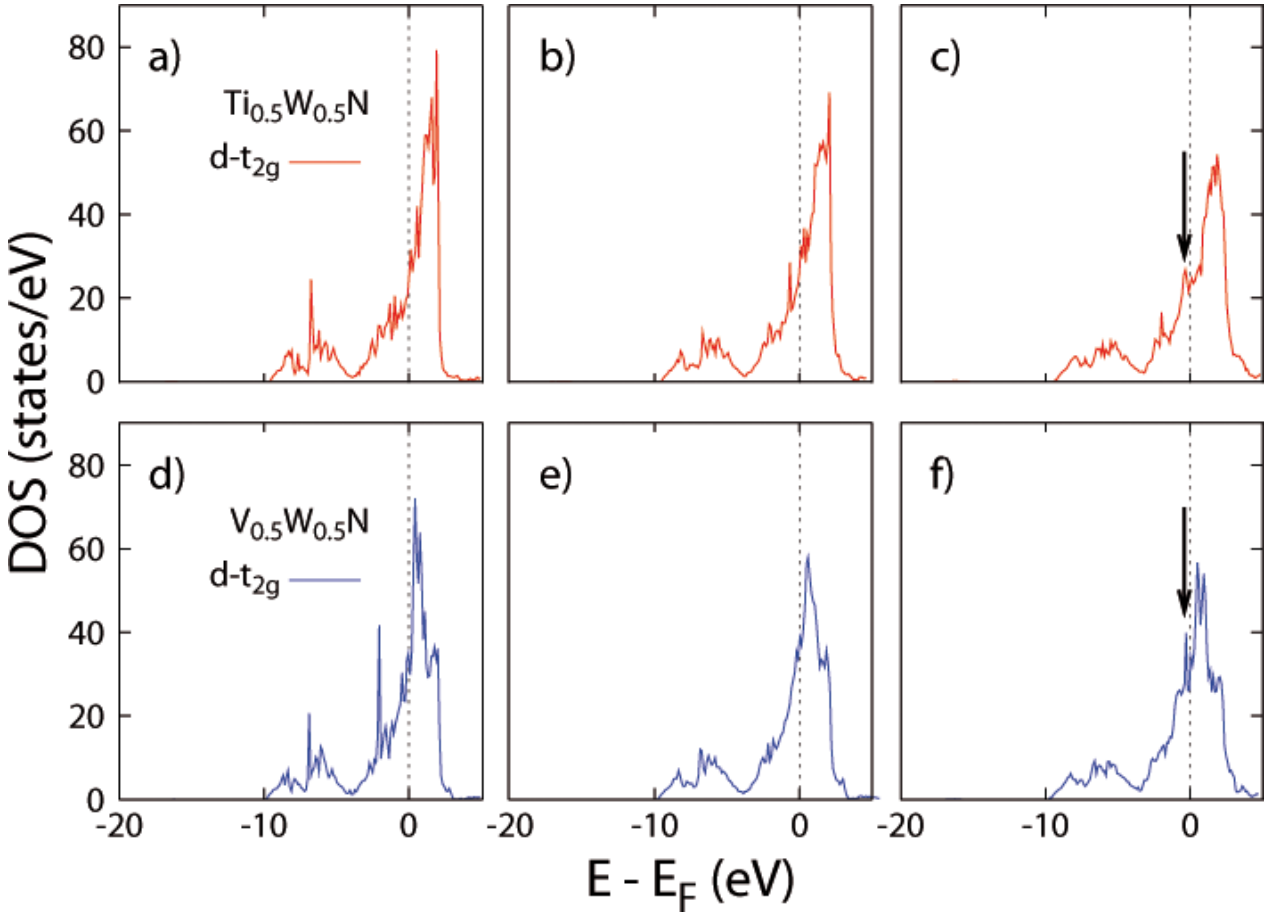

Fig. 4. (Color online) d-t_{2g} states response to shearing in $Ti_{0.5}W_{0.5}N$ (upper panels) and $V_{0.5}W_{0.5}N$ (lower panels) at increasing strains. From left to right, each series of panels (a-c), respectively (d-f), corresponds to 0, 5 and 10% strains.

Qualitatively, identical changes are induced with increasing strain in the covalent character of bonding in $V_{0.5}W_{0.5}N$, as shown by the COOP results obtained from the overlapping of the same orbitals as those for $Ti_{0.5}W_{0.5}N$. These are presented in Fig. 6, where one can clearly observe that 1st neighbor interactions, p – d bonds, are weakened upon shearing (top panels), while 2nd neighbor interactions, d – d bonds, become considerably stronger (lower panels) at higher strains. The overall trend of covalent bonding in the crystals can be assessed from our integrated COOP (ICOOP) results, which are shown in Fig. 7

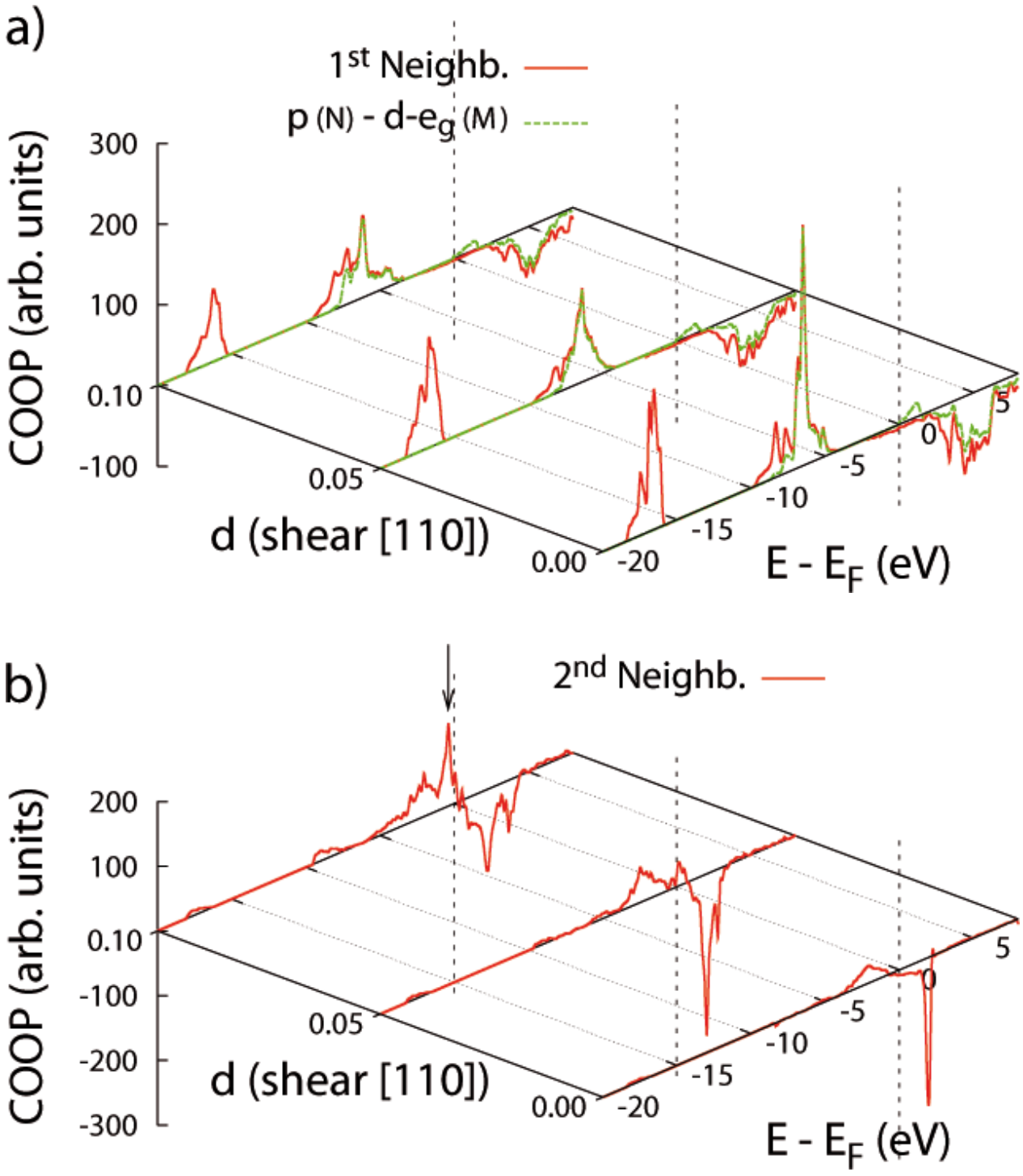

Fig. 5. (Color online) COOP effects induced by shearing at 0, 5 and 10% strains, resolved in first and second neighbor orbital interactions, in $Ti_{0.5}W_{0.5}N$: (a) progressive weakening of the covalent character of first neighbor N – *M* bonds; (b) corresponding gradual increase in covalent bonding in second neighbor *M* – *M* interactions.

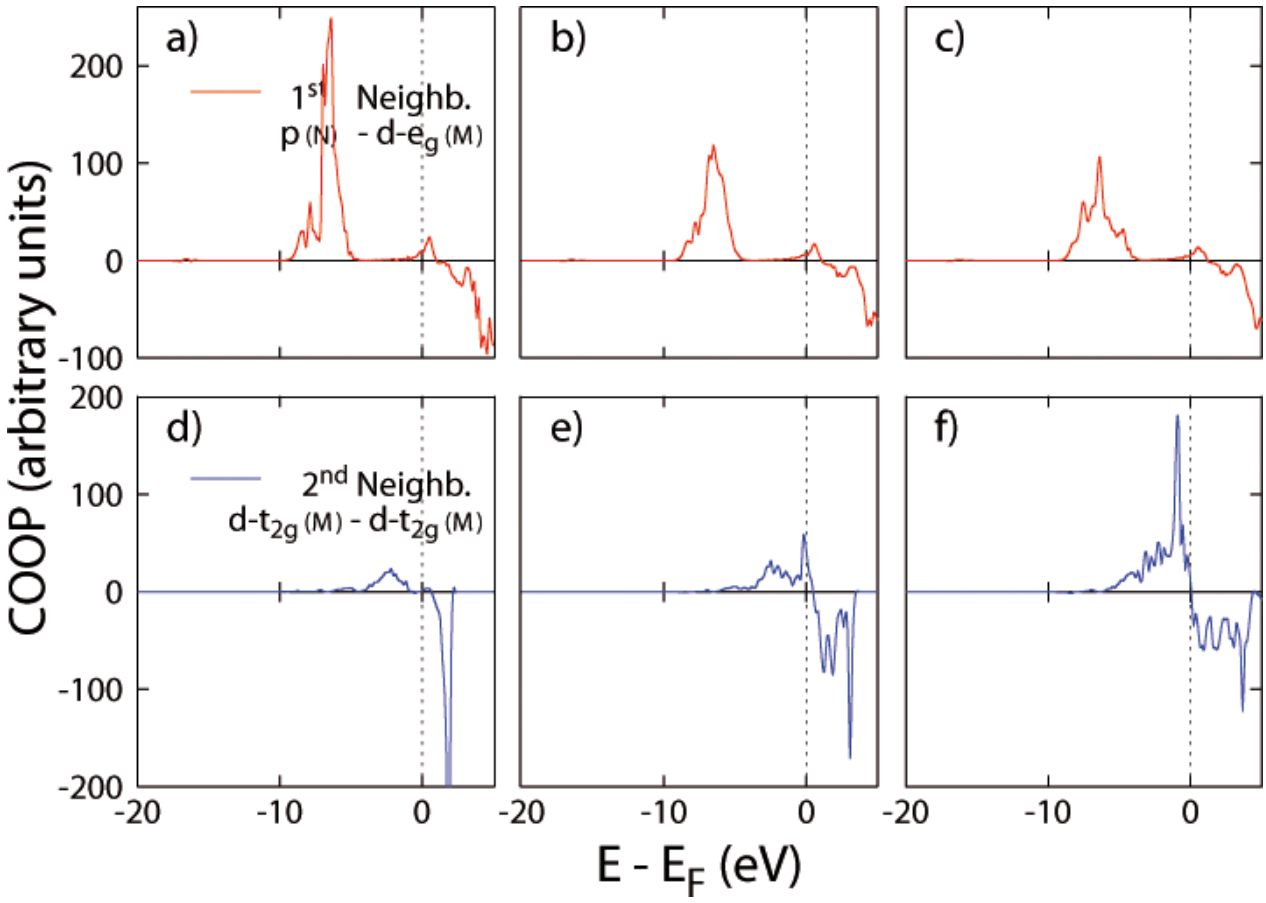

Fig. 6. (Color online) COOP analysis for $V_{0.5}W_{0.5}N$, resolved in first neighbor (upper panels) and second neighbor (lower panels) orbital interactions. From left to right, each series of panels (a-c), respectively (d-f), corresponds to 0, 5 and 10% strains.

(actual values in Table 5). Once again, the similarity between $Ti_{0.5}W_{0.5}N$ (Figs. 7a-7c) and $V_{0.5}W_{0.5}N$ (Figs. 7d-7f) is obvious, with respect to the dependence of 1st and 2nd neighbor interactions on the applied strain.

These results also clarify the role played by the additional electron per unit cell in orbitals overlapping in the ternaries. For illustrative purposes, a schematic representation of orbitals interaction in unstrained and strained configurations, is given in Fig. 8, where we show the typical 1st (Figs. 8a and 8b), respectively 2nd (Figs. 8c and 8d), neighbors orbitals arrangement. As it can be seen, upon shearing, for 1st neighbors *p* – *d* orbitals the overlapping region decreases, while for the 2nd neighbors *d* – *d* orbitals it increases. Naturally, this situation holds for both binaries and ternaries, but the additional electron per unit cell in

ternaries plays the decisive role, leading to significantly more $d - d$ orbitals overlapping and filling of the d-t_{2g} states. This observation is confirmed by the ICOOP results for binaries shown in Fig. 9 (actual values in Table 5), in which the absolute values at Fermi levels obtained for 2nd neighbor interactions are considerably lower than for the ternaries, shown in Fig. 7.

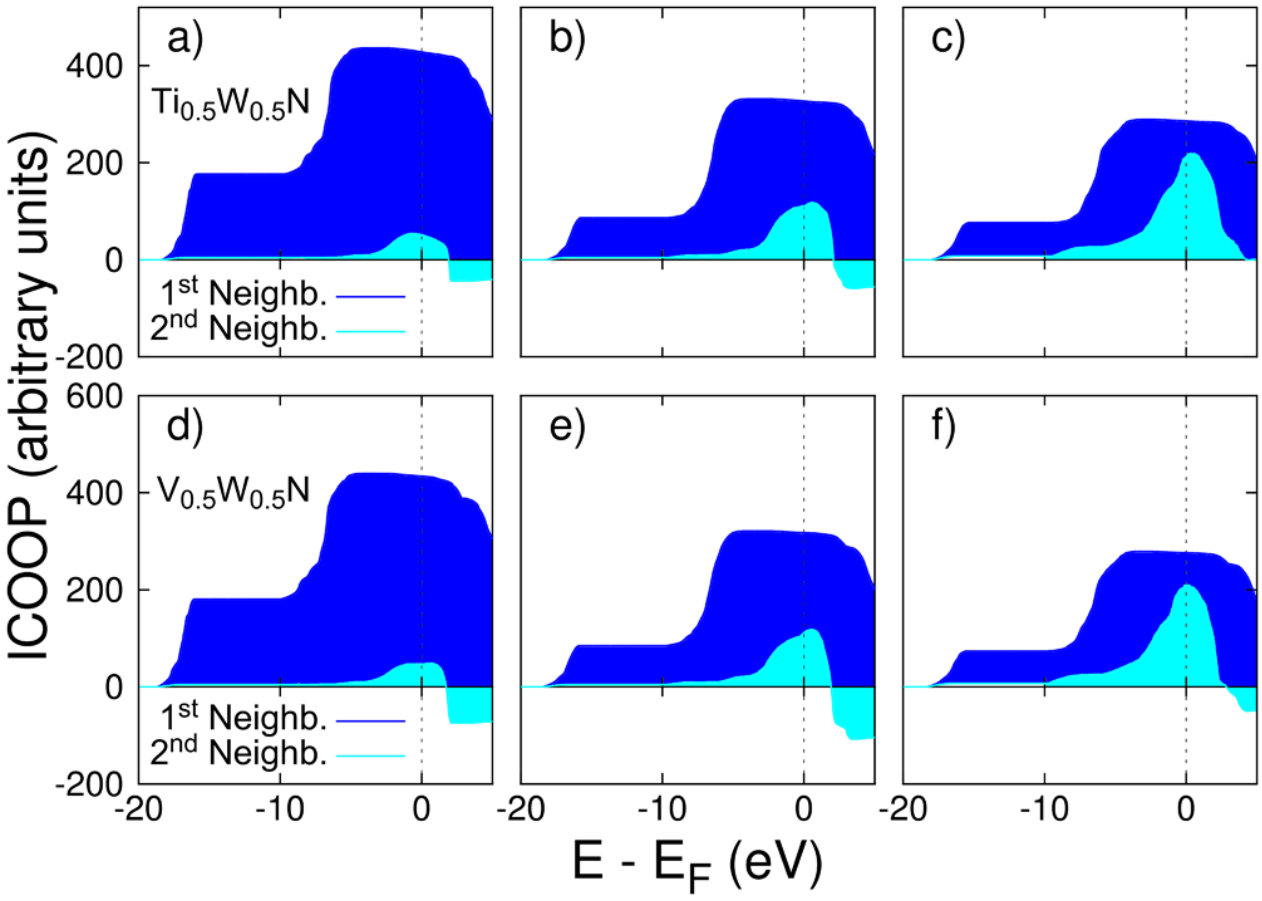

Fig. 7. (Color online) Integrated COOP (ICOOP) analysis for $Ti_{0.5}W_{0.5}N$ (upper panels) and $V_{0.5}W_{0.5}N$ (lower panels). From left to right, each series of panels (a-c), respectively (d-f), corresponds to 0, 5 and 10% strains. ICOOP values at the Fermi level indicate the covalent bond strength.

Nevertheless, bonding in these compounds is not entirely covalent, and so one needs to go beyond a COOP analysis in order to assess other significant changes induced by strain in the bonding of these materials. To achieve this task, we map the difference between the self-

Table 5. Integrated COOP (ICOOP) values, in arbitrary units, showing bond strength at Fermi level and applied shear strains, for 1st and 2nd neighbor orbital overlapping.

Strain [%]	1st neighb.			2nd neighb.		
	0	5	10	0	5	10
TiN	352	191	168	35	48	82
VN	334	268	233	33	74	132
$Ti_{0.5}W_{0.5}N$	428	327	286	51	110	212
$V_{0.5}W_{0.5}N$	434	318	276	47	112	209

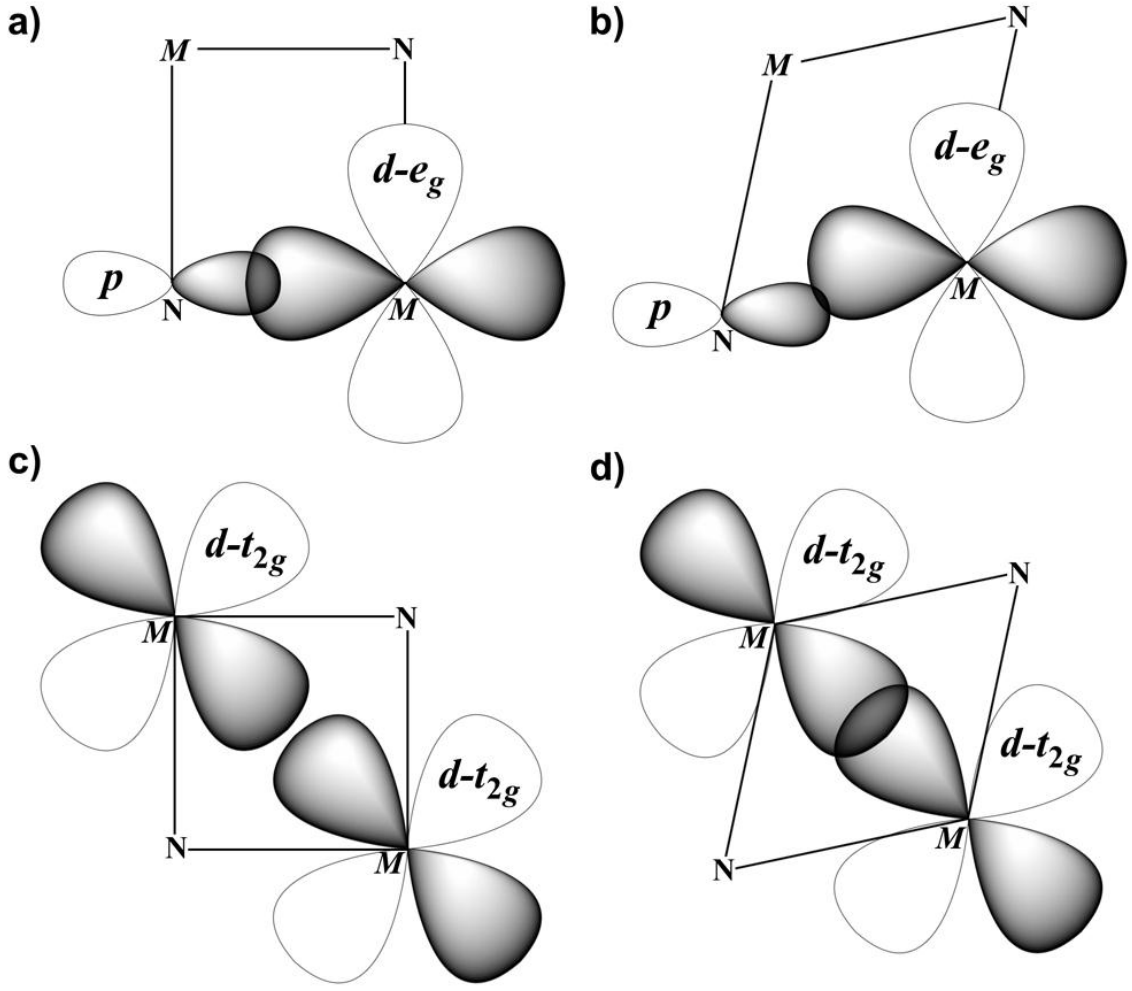

Fig. 8. Schematic representation of first and second neighbor orbitals overlapping in unstrained and shear strained B1 transition metal nitrides. Any existing p – d-e_g, first neighbor orbitals, overlapping in unstrained structures (a) decreases with applied strains (b). The opposite situation is observed for second neighbor d-t_{2g} – d-t_{2g} orbitals, when overlapping is significantly enhanced during shearing deformations, (c) and (d).

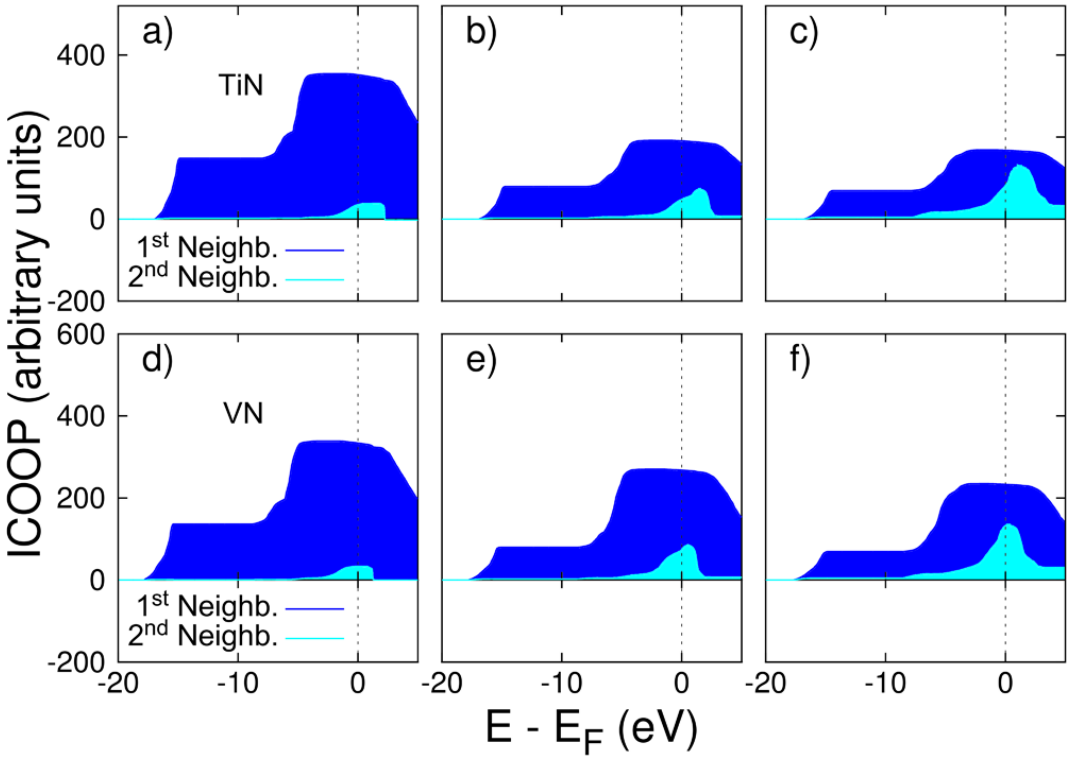

Fig. 9. (Color online) Integrated COOP (ICOOP) analysis for TiN (upper panels) and VN (lower panels). From left to right, each series of panels (a-c), respectively (d-f), corresponds to 0, 5 and 10% strains.

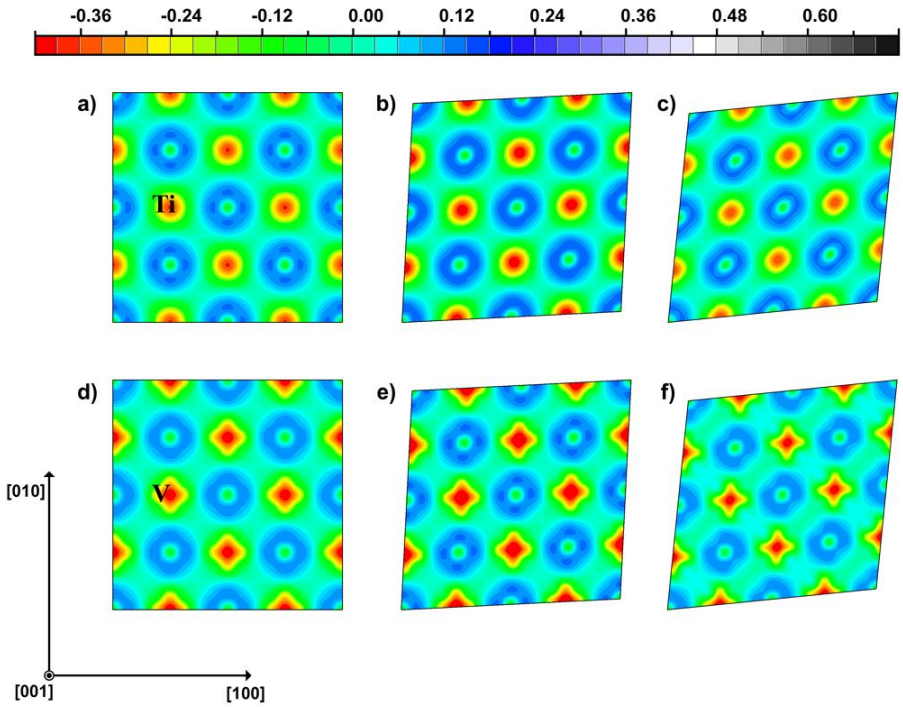

Fig. 10. (Color online) Charge density difference maps for TiN (upper panels) and VN (lower panels), and effects of shearing applied on the (001) plane. From left to right, each series of panels (a-c), respectively (d-f), corresponds to 0, 5 and 10% strains. Color scale units are electrons/Å^3.

consistent electron density and the atomic charge density on the (001) plane. This technique allows tracing electrons migration from an initially unperturbed atomic arrangement into the chemical bonds of the final crystal structure, i.e. changes with both ionic and covalent character induced by strain. These results are shown in Fig 10 for TiN (top panels), and VN (lower panels), respectively in Fig. 11 for $Ti_{0.5}W_{0.5}N$ (top panels) and $V_{0.5}W_{0.5}N$ (lower panels). In all four compounds, valence electrons partially transfer from the metal atomic shells to neighboring N atoms to form $p - d$ ionic-covalent bonds. In TiN and $Ti_{0.5}W_{0.5}N$ (Figs. 10a and 11a), Ti-N bonds have a pronounced ionic character, as implied by the spherical charge distribution surrounding the atoms. In VN and $V_{0.5}W_{0.5}N$ on the other hand, the clear square-ish charge distribution surrounding V atoms shows that V-N bonds are more directional (Figs. 10d and 11d). In both ternaries, W-N bonds have a distinct directional character, as evidenced by the four lobes pointing towards neighboring N (Figs. 11a and 11d), in agreement with plots in Figs. 2a and 2c. In this instance, however, it is important to note the significant transfer of charge from W atoms towards N atoms (compare Fig. 10a with 11a, respectively 10d with 11d). This effect is visible in both ternaries but especially in $V_{0.5}W_{0.5}N$, where the well defined moon-like shapes in the charge difference map, in the vicinity of N atoms, clearly prove the existence of this charge transfer (Fig. 11d). Thus, these results demonstrate that alloying affects the electronic structure of binaries, as it induces a charge migration process which yields in ternaries stronger ionic, implicitly shorter, N – Ti/V bonds, and weaker/longer W-N bonds.

It is then interesting to note the changes induced by shearing upon both sets of compounds. In binaries, one can clearly observe that as strain increases, charge is being smeared in between constituent atoms along the [110] direction of applied trigonal strain, as evidenced by the elongated charge shapes surrounding atoms in this direction (Figs. 10b and 10c, TiN, respectively 10e and 10f, VN). Clearly, binaries resist shearing essentially in an

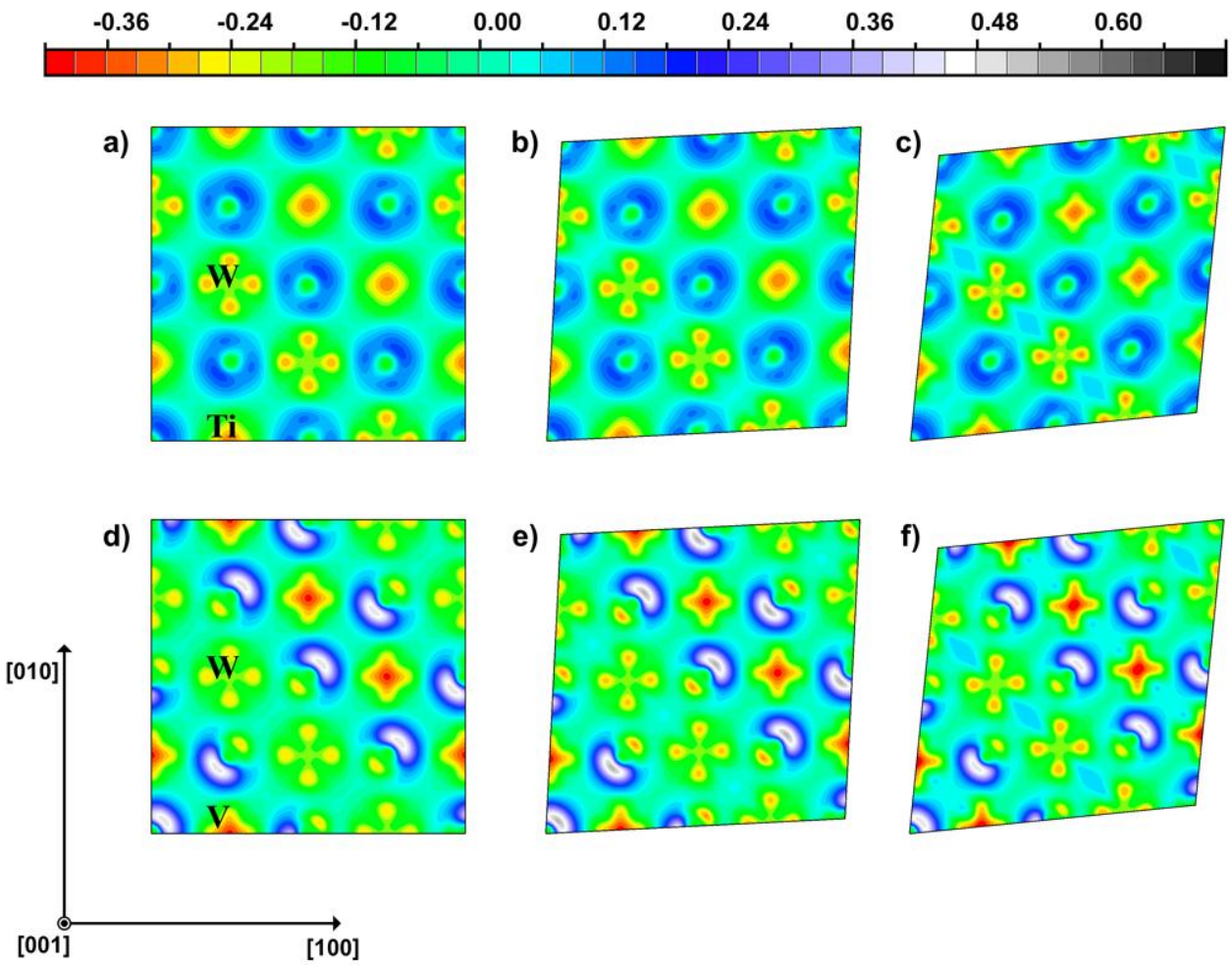

Fig. 11. (Color online) Charge density difference maps for $Ti_{0.5}W_{0.5}N$ (upper panels) and $V_{0.5}W_{0.5}N$ (lower panels), and effects of shearing applied on the (001) plane. From left to right, each series of panels (a-c), respectively (d-f), corresponds to 0, 5 and 10% strains. Color scale units are electrons/$Å^3$.

ionic manner, and as atoms are pulled apart, there is also a tendency to somewhat increase directional/covalent bonding in the direction of the applied strain, as evidenced by the widening (light blue online) channels of charge transfer in this direction. To some extent, similar changes can be observed in the ternaries (Figs. 11b and 11c, $Ti_{0.5}W_{0.5}N$, respectively, 11e and 11f, $V_{0.5}W_{0.5}N$). In this case, however, the most significant, clearly visible change is the appearance of well contoured, oriented lobes of positive charge transfer (darker blue online) between the W atoms. The presence of these lobes demonstrates a significant increase

in directional/covalent bonding along the W-W stacking planes, which equates to a considerable strengthening of metal-metal bonds in the $[1\,\bar{1}\,0]$ direction, perpendicular to that of the applied strain. This result is consistent with the shearing induced formation of a layered electronic structure reported for Ti nitrides [15], and fully supports our analysis of other ternaries considered in this study.

In addition to the arguments presented so far in this study, the following rational helps to further elucidate the mechanism through which ductility is promoted and enhanced in these ternaries. Upon replacing Ti/V atoms with W in TiN/VN, and forming the close to experimental observations [29] C#3 configuration, the lattice point symmetry is reduced from O_h into C_{3v}. In this configuration, N is coordinated with Ti/V and W on opposite verses of each Cartesian direction. The electronic environment anisotropy leads to a relaxation of N atomic positions, and the displacement of N atoms from ideal B1 lattice sites depends on the relative bonding strengths with neighboring atoms. As showed in the preceding sections, the N – Ti/V bonds are stronger than W-N bonds, so the B1 $\rightarrow$ C#3 transition will yield a shortening of the Ti/V – N distances. This trend will be enhanced with increasing strain, as shown in Fig. 12 where we plot the bond length ratios of the W– N bonds with respect to Ti/V – N bonds in the two ternaries.

At the same time, one should consider the well known fact that one of main channels for dislocations glide at low temperatures in B1-nitrides is the $\{110\}\langle 1\,\bar{1}\,0\rangle$ slip system [1]. During dislocations motion, bonds are broken and reformed, and obviously dislocations glide will occur more easily in planes normal to those containing weaker bonds. In the nitrides considered here this is clearly the case. In addition to the demonstrated weaker bonding between the W-N planes induced in the B1 $\rightarrow$ C#3 transition, the [110] trigonal deformation was shown to yield stronger covalent bonding along the $[1\,\bar{1}\,0]$ W-W planes. At a certain

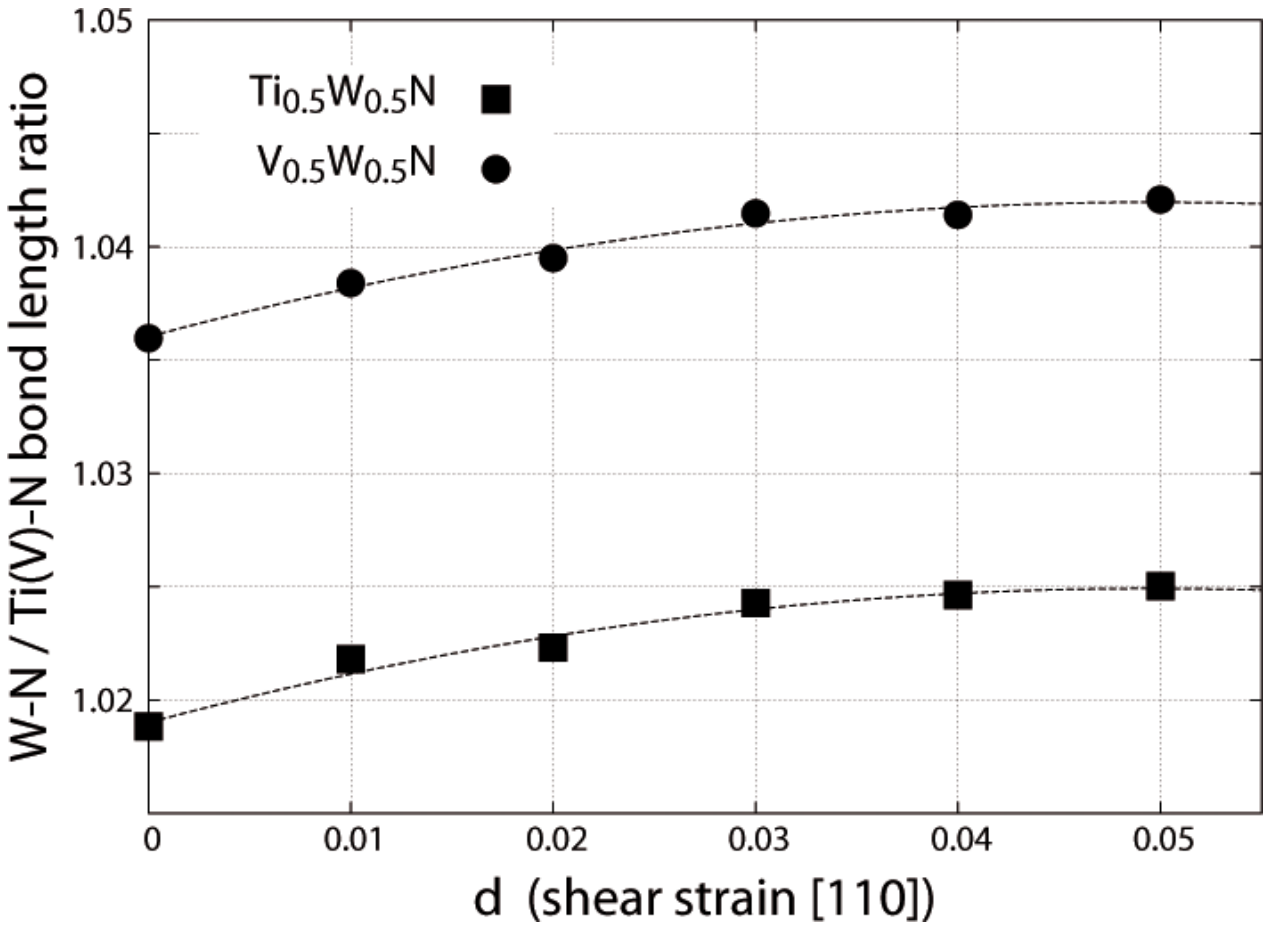

Fig. 12. Bond length ratio dependence on strain: W-N/Ti-N bonds in $Ti_{0.5}W_{0.5}N$ (black squares) and W-N/V-N bonds in $V_{0.5}W_{0.5}N$ (black circles).

level of shearing strain, this set of conditions will obviously favor the breakage of bonds between W-N atomic planes, allow these planes to slide against each other, and make the $\{110\}\langle 1\bar{1}0\rangle$ slip system a primary channel for dislocations glide. Equally important, during dislocations glide, the strong covalent bonding within W-W slip planes will further delay bond snapping. These are the key mechanisms which promote and enhance ductility in these ternaries. This is not, however, the situation in TiN and VN, where, as it was shown, the Ti/V – N bonds are equally robust in all planes and resist any type of deformation, tetragonal or trigonal strains, thus explaining their hardness as well as their brittleness. These arguments are clearly supported by our analysis of the stress-strain relationship in TiN, VN and corresponding W-alloyed ternaries, as shown in Fig. 13. As it can be seen, the binaries are

characterized by a definite linear-elastic response to shearing, while the ternaries exhibit a visibly more plastic stress-strain response to deformations.

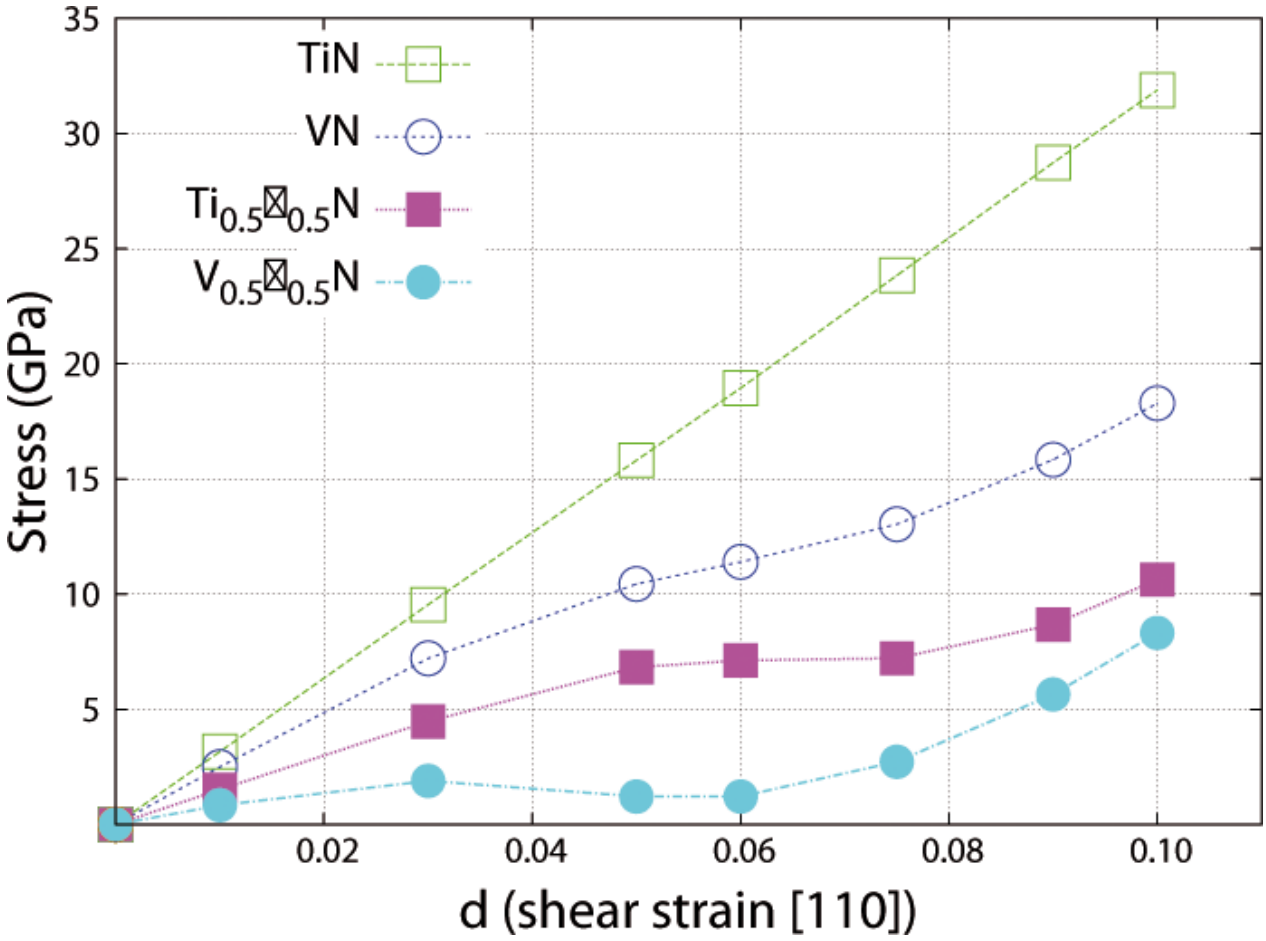

Fig. 13. (Color online) Calculated stress – strain trends in TiN (green, open squares), VN (blue, open circles), $Ti_{0.5}W_{0.5}N$ (red, solid squares) and $V_{0.5}W_{0.5}N$ (blue, solid circles).

As mentioned in the preceding sections of this study, the findings reported for $Ti_{0.5}W_{0.5}N$ and $V_{0.5}W_{0.5}N$ are expected to be valid for the other alloying combinations considered herein, as these were shown to be in fact a VEC induced effect. The trend in ductility criteria is clearly illustrated in Fig. 14, for both Ti and V based ternary nitrides. Therein, we also include as a reference point the results for $Ti_{0.5}Al_{0.5}N$, compound with a VEC of 8.5 electrons per unit cell, i.e. marginally higher than the threshold of 8.4 for which maximum hardness is expected. The VEC dependence, consisting in decreasing *G*/*B* ratios (Fig. 14a) and

increasingly positive values of Cauchy pressures (C_{12}-C_{44}) (Fig. 14b) is obvious for all ternaries considered in this study. A similar effect is somewhat active in binaries, as VN is shown to have more ductile properties compared to TiN, though clearly not as pronounced as in the case of ternaries.

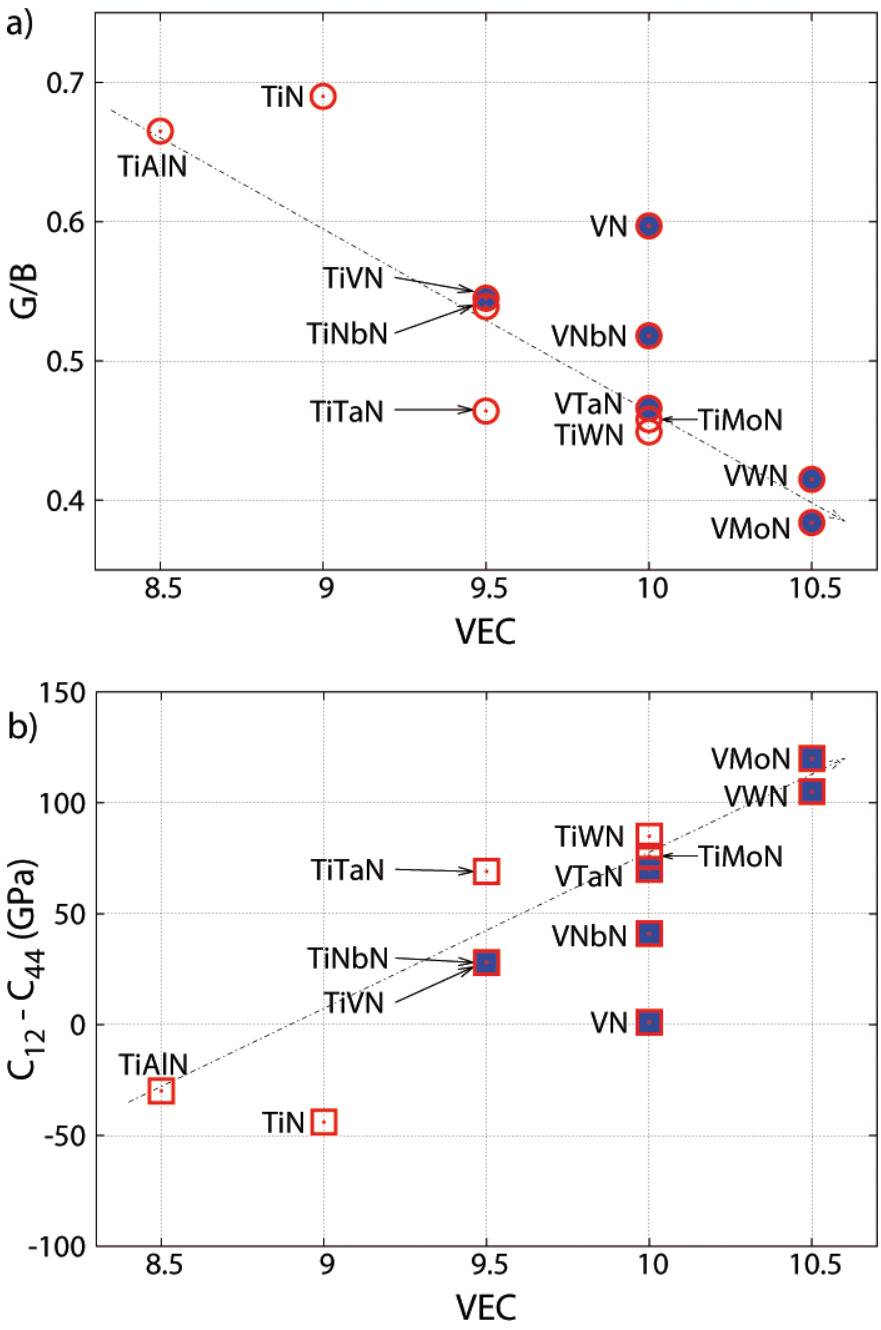

Fig. 14. (Color online) VEC induced trends in Ti and V based B1 transition metal nitrides. (a) G/B ratios dependence on VEC; Ti (red, open circles) and V (blue, solid circles) nitrides; (b) VEC effect on Cauchy pressures in Ti (red, open squares), and V (blue, solid squares) compounds.

4. Conclusions

Our DFT calculations predict the existence and explain the origins of supertoughening in cubic-B1 Ti and V ternary nitrides obtained by alloying TiN and VN with Nb, Ta, Mo, and W in 50% concentrations. All ternaries considered in this study are predicted to have hardness values at least comparable to the reference binaries and significantly enhanced ductile characteristics. This phenomenon is shown to be primarily an effect of increased VEC per unit cell, equating to stronger reference metal Ti/V-N, respectively weaker alloying metal Nb/Ta/Mo/W – N bonds, which upon shearing yields an increased occupancy of d-t_{2g} metallic states. This combination of properties leads to the formation of a layered electronic structure, and ultimately allows a selective response to strain and shear deformations by assisting the activation of the $\{110\}\langle 1\bar{1}0\rangle$ slip system for dislocations glide.

Acknowledgements

The work was supported by the Swedish Research Council (VR) and the Swedish Strategic Research Foundation (SSF) Program on Materials Science and Advanced Surface Engineering. All calculations were performed on the Neolith and the Kappa clusters located at the National Supercomputer Centre (NSC) in Linköping.

References

[1] Toth LE. Transition Metal Carbides and Nitrides. New York: Academic Press, 1971.

[2] Howe BM, Sammann E, Wen JG, Spila T, Greene JE, Hultman L, Petrov I. Acta Mater 2011;59:421.

[3] Mayrhofer PH, Fischer FD, Bohm HJ, Mitterer C, Schneider JM. Acta Mater 2007;55:1441.

[4] Zhitomirsky VN. Surf Coat Technol 2007;201:6122.

[5] Cavaleiro A, Trindade B, Vieira MT. Surf Coat Technol 2003;174:68.

[6] Yang Q, Zhao LR, Patnaik PC, Zeng XT. Wear 2006;261:119.

[7] Latella BA, Gan BK, Davies KE, McKenzie DR, McCulloch DG. Surf Coat Technol 2006;200:3605.

[8] Yang JF, Yuan ZG, Zhang GG, Wang XP, Fang QF. Mater Res Bull 2009;44:1948.

[9] Hugosson HW, Jansson U, Johansson B, Eriksson O. Science 2001;293:2434.

[10] Joelsson T, Hultman L, Hugosson HW, Molina-Aldareguia JM. Appl Phys Lett 2005;86:131922.

[11] Madan A, Wang YY, Barnett SA, Engstrom C, Ljungcrantz H, Hultman L, Grimsditch M. J Appl Phys 1998;84:776.

[12] Voevodin AA, Zabinski JS. Thin Solid Films 2000;370:223.

[13] Chen KY, Zhao LR, Rodgers J, Tse JS. J Phys D: Appl Phys 2003;36:2725.

[14] Zhao LR, Chen K, Yang Q, Rodgers JR, Chiou SH. Surf Coat Technol 2005;200:1595.

[15] Sangiovanni DG, Chirita V, Hultman L. Phys Rev B 2010;81:104107.

[16] Weast RC. Handbook of Chemistry and Physics, 57th ed.: CRC Press, 1976.

[17] Wiemer C, Sanjines R, Levy F. Surf Coat Technol 1996;86:372.

[18] Freller H, Lorenz HP, Schack P. Surf Coat Technol 1992;54:148.

[19] Sanjines R, Wiemer C, Hones P, Levy F. J Appl Phys 1998;83:1396.

[20] Kim BJ, Lee SH, Lee JJ. J Mater Sci Lett 1997;16:1597.

[21] Suetin DV, Shein IR, Ivanovskii AL. Phys Status Solidi B 2008;245:1590.

[22] Hoffmann R. Solids and Surfaces: A Chemist's View of Bonding in Extended Structures: Wiley-VCH, 1988.

[23] Šimůnek A. Phys Rev B 2007;75:172108.

[24] Guo X, Li L, Liu Z, Yu D, He J, Liu R, Xu B, Tian Y, Wang HT. J Appl Phys 2008;104:023503.

[25] Kresse G, Hafner J. Phys Rev B 1994;49:14251.

[26] Perdew JP, Wang Y. Phys Rev B 1992;45:13244.

[27] Blöchl PE. Phys Rev B 1994;50:17953.

[28] Monkhorst HJ, Pack JD. Phys Rev B 1976;13:5188.

[29] Tian F, D'Arcy-Gall J, Lee TY, Sardela M, Gall D, Petrov I, Greene JE. J Vac Sci Technol A 2003;21:140.

[30] Birch F. J Geophys Res 1978;83:1257.

[31] Pearson WB. The Crystal Chemistry and Physics of Metals and Alloys. New York: Wiley, 1972.

[32] Gao F, He J, Wu E, Liu S, Yu D, Li D, Zhang S, Tian Y. Phys Rev Lett 2003;91:015502.

[33] Roundy D, Krenn CR, Cohen ML, Morris JW. Phys Rev Lett 1999;82:2713.

[34] Lee T, Ohmori K, Shin CS, Cahill DG, Petrov I, Greene JE. Phys Rev B 2005;71:144106.

[35] Kim JO, Achenbach JD, Mirkarimi PB, Shinn M, Barnett SA. J Appl Phys 1992;72:1805.

[36] Peng ZJ, Miao HZ, Qi LH, Yang S, Liu CZ. Acta Mater 2003;51:3085.

[37] Shinn M, Barnett SA. Appl Phys Lett 1994;64:61.

[38] Mirkarimi PB, Shinn M, Barnett SA, Kumar S, Grimsditch M. J Appl Phys 1992;71:4955.

[39] Ahuja R, Eriksson O, Wills JM, Johansson B. Phys Rev B 1996;53:3072.

[40] Nagao S, Nordlund K, Nowak R. Phys Rev B 2006;73:144133.

[41] Lazar P, Redinger J, Podloucky R. Phys Rev B 2007;76:174112.

[42] Isaev EI, Simak SI, Abrikosov IA, Ahuja R, Vekilov YK, Katsnelson MI, Lichtenstein AI, Johansson B. J Appl Phys 2007;101:123519.

[43] Siegel DJ, Hector LG, Adams JB. Acta Mater 2002;50:619.

[44] Matenoglou GM, Koutsokeras LE, Lekka CE, Abadias G, Kosmidis C, Evangelakis GA, Patsalas P. Surf Coat Technol 2009;204:911.

[45] Sanjines R, Wiemer C, Almeida J, Levy F. Thin Solid Films 1996;291:334.

[46] König U. Surf Coat Technol 1987;33:91.

[47] Abadias G. Surf Coat Technol 2008;202:2223.

[48] Abadias G, Koutsokeras LE, Dub SN, Tolmachova GN, Debelle A, Sauvage T, Villechaise P. J Vac Sci Technol A 2010;28:541.

[49] Šimůnek A, Vackář J. Phys Rev Lett 2006;96:085501.

[50] Liu ZY, Guo X, He J, Yu D, Tian Y. Phys Rev Lett 2007;98:109601.

[51] Šimůnek A, Vackář J. Phys Rev Lett 2007;98:109602.

[52] Huang CT, Duh JG. Surf Coat Technol 1995;71:259.

[53] Mirkarimi PB, Hultman L, Barnett SA. Appl Phys Lett 1990;57:2654.

[54] Shin CS, Gall D, Hellgren N, Patscheider J, Petrov I, Greene JE. J Appl Phys 2003;93:6025.

[55] Shaginyan LR, Misina M, Zemek J, Musil J, Regent F, Britun VF. Thin Solid Films 2002;408:136.

[56] Wang Y, Tam PL, Shen YG. Thin Solid Films 2008;516:7641.

[57] Farges G, Beauprez E, Stecatherine MC. Surf Coat Technol 1993;61:238.

[58] Ljungcrantz H, Engstrom C, Hultman L, Olsson M, Chu X, Wong MS, Sproul WD. J Vac Sci Technol A 1998;16:3104.

[59] Helmersson U, Todorova S, Barnett SA, Sundgren JE, Markert LC, Greene JE. J Appl Phys 1987;62:481.

[60] Pugh SF. Philos Mag 1954;45:823.

[61] Pettifor DG. Mater Sci Technol 1992;8:345.

[62] Jhi SH, Ihm J, Louie SG, Cohen ML. Nature 1999;399:132.

[63] Magnuson M, Mattesini M, Li S, Hoglund C, Beckers M, Hultman L, Eriksson O. Phys Rev B 2007;76:195127.